Redox Biology 45 (2021) 102040

Contents lists available at ScienceDirect

Redox Biology

journal homepage: www.elsevier.com/locate/redox

Duchenne's muscular dystrophy involves a defective transsulfuration pathway activity

E. Panza [a,1], V. Vellecco [a,1], F.A. Iannotti [b], D. Paris [b], O.L. Manzo [a,c], M. Smimmo [a], N. Mitilini [d], A. Boscaino [d], G. de Dominicis [d], M. Bucci [a,*], A. Di Lorenzo [c], G. Cirino [a]

[a] Department of Pharmacy, School of Medicine and Surgery, University of Naples Federico II, Naples, Italy
[b] Institute of Biomolecular Chemistry (ICB), National Research Council (CNR), Pozzuoli (NA), Italy
[c] Center for Vascular Biology, Department of Pathology and Laboratory Medicine, Weill Cornell Medical College, Cornell University, New York, NY, USA
[d] UOSC, Pathological Anatomy, A. Cardarelli Hospital, Naples, Italy

ARTICLE INFO

Keywords:
H_2S donors
Sodium hydrosulfide (NaHS)
Duchenne muscular dystrophy
Autophagy
Inflammation

ABSTRACT

Duchenne muscular dystrophy (DMD) is the most frequent X chromosome-linked disease caused by mutations in the gene encoding for dystrophin, leading to progressive and unstoppable degeneration of skeletal muscle tissues. Despite recent advances in the understanding of the molecular processes involved in the pathogenesis of DMD, there is still no cure. In this study, we aim at investigating the potential involvement of the transsulfuration pathway (TSP), and its by-end product namely hydrogen sulfide (H_2S), in primary human myoblasts isolated from DMD donors and skeletal muscles of dystrophic (*mdx*) mice. In myoblasts of DMD donors, we demonstrate that the expression of key genes regulating the H_2S production and TSP activity, including cystathionine γ lyase (CSE), cystathionine beta-synthase (CBS), 3 mercaptopyruvate sulfurtransferase (3-MST), cysteine dioxygenase (CDO), cysteine sulfonic acid decarboxylase (CSAD), glutathione synthase (GS) and γ -glutamylcysteine synthetase (γ-GCS) is reduced. Starting from these findings, using Nuclear Magnetic Resonance (NMR) and quantitative Polymerase Chain Reaction (qPCR) we show that the levels of TSP-related metabolites such as methionine, glycine, glutathione, glutamate and taurine, as well as the expression levels of the aforementioned TSP related genes, are significantly reduced in skeletal muscles of *mdx* mice compared to healthy controls, at both an early (7 weeks) and overt (17 weeks) stage of the disease. Importantly, the treatment with sodium hydrosulfide (NaHS), a commonly used H_2S donor, fully recovers the impaired locomotor activity in both 7 and 17 old *mdx* mice. This is an effect attributable to the reduced expression of pro-inflammatory markers and restoration of autophagy in skeletal muscle tissues. In conclusion, our study uncovers a defective TSP pathway activity in DMD and highlights the role of H_2S-donors for novel and safe adjuvant therapy to treat symptoms of DMD.

1. Introduction

Duchenne muscular dystrophy (DMD) is the most frequent form of skeletal muscle (SKM) dystrophy characterized by a rapid weakening and functional failure of skeletal muscles. It affects up to 1 in every 5000 live male birth [1]. Mutations and/or deletions in the X-linked gene encoding for dystrophin are the causes of the disease. In skeletal and cardiac muscle, dystrophin is part of the dystrophin-associated protein (DAPC) complex, acting to connect the cytoskeleton of muscle fiber to the extracellular matrix, thus stabilizing the sarcolemma during repeated cycles of contraction and relaxation [2,3]. Consequently, the lack of functional dystrophin causes the breakdown of muscle tissue leading to rapid and progressive tissue degeneration. The reiterated local damage, coupled with chronic inflammation and muscle necrosis, leads to reduced myofibers regeneration that is progressively replaced by connective and adipose tissues [4–6]. Additionally, increasing lines of evidence demonstrate that autophagy, a key cellular process required for the removal of unnecessary or dysfunctional organelles and components, is severely impaired in DMD. Thus, restoration of functional autophagy is believed one of the most promising strategies to reinforce

* Corresponding author. Department of Pharmacy, School of Medicine and Surgery, University of Naples Federico II, via D. Montesano 49, 80131, Naples, Italy.
E-mail address: mrbucci@unina.it (M. Bucci).
[1] These authors contributed equally to this work.

https://doi.org/10.1016/j.redox.2021.102040
Received 12 February 2021; Received in revised form 20 May 2021; Accepted 7 June 2021
Available online 19 June 2021

DMD muscle regeneration and function [7–9]. Despite several experimental approaches aimed to restore and/or compensate the dystrophin deficit have been proposed, to date, there is no cure for this disease.

Hydrogen sulfide (H_2S) is a ubiquitous small gaseous mediator and its regulation and action are tightly linked to the cellular homeostasis and maintenance of health [10,11]. In mammals, three enzymes are responsible for H_2S production: cystathionine γ-lyase (CSE), cystathionineβ-synthase (CBS), and 3-mercaptopyruvate sulfurtransferase (3-MST). CSE and CBS catalyze the de-sulfhydration of L-cysteine to generate H_2S, while 3-MST generates H_2S by modulating the activity of the cysteine aminotransferase (CAT) enzyme [12–15]. All three enzymes belong to the transsulfuration pathway (TSP), a complex multi-step pathway, which not only is deputed to the generation of H_2S from L-cysteine, but also leads to other key metabolites including glutathione (GSH) and L-taurine. In particular, the production of GSH from L-cysteine is driven by γ -glutamylcysteine synthetase (γ-GCS) and glutathione synthase (GS) enzymes; while L-taurine is produced by the subsequential action of other three enzymes named cysteine dioxygenase (CDO), cysteine sulfonic acid decarboxylase (CSAD) and hypotaurine dehydrogenase (HDD) (Fig. 1) [10,16,17]. In addition to its essential role in protein synthesis, L-cysteine is also a component of the major antioxidant GSH and a potent antioxidant itself. Disruption of L-cysteine and GSH metabolism has been frequently linked to aberrant redox homeostasis and neurodegeneration [18,19]. Taurine plays a role in osmoregulation, immunomodulation, neuromodulation, Ca^{2+} homeostasis, ocular function and possesses antioxidant and anti-inflammatory effects [20]. However, it is important to consider that excessive reductive stress could be detrimental as is oxidative stress in tissues, skeletal muscle and heart included [21]. The anti-inflammatory and anti-oxidant action of H_2S has been demonstrated in many types of human disorders [15,22,23] but its involvement in SKM diseases remains largely unknown. Recently, the role of the H_2S signalling in skeletal muscle has been investigated showing that H_2S biosynthesis is increased in Malignant Hyperthermia, a human syndrome characterized by an anomalous SKM hypercontractility following exposure to volatile anaesthetics, and this consequence contributes to the pathological hypercontractility observed [24,25]. Based on these pieces of evidence, this study aims to investigate the possible involvement of the TSP, and in particular H_2S, in the DMD.

2. Results

2.1. Measurement of TSP related genes in human primary myoblasts isolated from healthy and DMD donors

To gain information about the potential TSP involvement in DMD, using quantitative PCR (qPCR) we measured the mRNA expression levels of CBS, CSE, 3-MST, CDO, CSAD, GS and γ-GCS in primary human myoblasts isolated from healthy and DMD donors (ranging from 1- to 7-years-old, table S2). As shown in Fig. 2, myoblasts isolated from DMD donors (D1-D4) display a significantly lower expression of CSE, 3-MST, CDO and CSAD compared to control cells isolated from healthy donors (HD1 and HD2). In contrast, CBS and GS genes are reduced only in D3 and D4, whereas γ-GCS gene does not show significant changes among samples (Fig. 2). Considering that the rapid and growing development of next-generation sequencing (NGS) technologies performed on blood lymphocytes has led to a strong reduction of the skeletal muscle biopsy to diagnose genetic disorders. [26–28], our results, although obtained from a limited number of human cells, could lead to the identification of unpredicted molecular mechanisms underlying the DMD pathophysiology, that could open novel therapeutic strategies. Therefore, based on these results, this study has been carried out in *mdx* mice, which represent one of the widely used animal models to perform preclinical studies on DMD recapitulating the major features of human disease.

2.2. Skeletal muscle of mdx mice displays a significant reduction in metabolites content related to the TSP pathway

To define the potential role of TSP activity in the ineffective repair and progressive degeneration of SKM occurring in DMD, an NMR-based metabolomics analysis in muscle tissues of control and *mdx* mice has been performed. Fig. 3A shows the pattern of distribution of the whole class of metabolites detected in quadriceps (QFA) muscle of both strains at 7 weeks of age. These data have been simplified by the Principal Coordinate Analysis (PCoA; Fig. S1) which emphasizes the dissimilarity between the two murine genotypes (wt vs *mdx*). Among many metabolites, the attention has been focused on the key metabolites known to regulate the TSP activity including methionine, L-glycine, L-glutamate, GSH and L-taurine. The analysis reveals that in *mdx* mice, the levels of all the metabolites selected are significantly reduced compared to control mice (Fig. 3B – F). The same analysis, performed at 17-weeks of age, instead shows a different pattern (Fig. 4A) a reversal of L-glycine and L-glutamate levels, which results in significantly higher in *mdx* compared

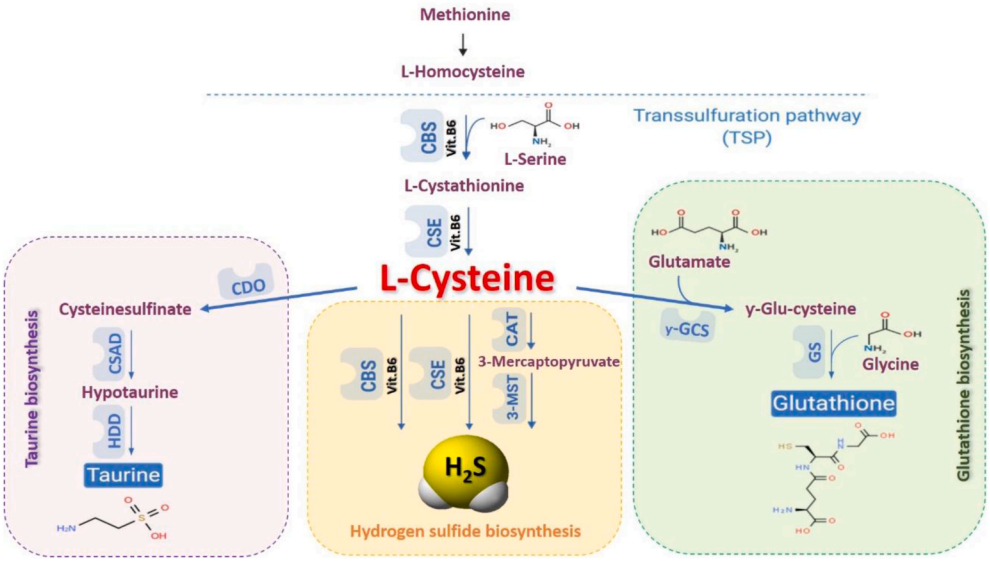

Fig. 1. Scheme of transsulfuration pathway (TSP). In mammalians, the amino acid methionine could be converted into homocysteine. Homocysteine could be transformed, through two steps enzymatic reaction, into L-cysteine. L-cysteine acts as a substrate leading to the biosynthesis of three major final products: H_2S, taurine and glutathione. Abbreviation: CAT, cysteine aminotransferase; CBS, cystathionine beta-synthase; CDO cysteine dioxygenase; CSAD, cysteine sulfonic acid decarboxylase; CSE, cystathionine-γ-lyase; GS: glutathione synthase; HDD, hypotaurine dehydrogenase; MPST, 3-mercaptopyruvate sulfurtransferase; γ-GCS: Gamma-glutamylcysteine synthetase.

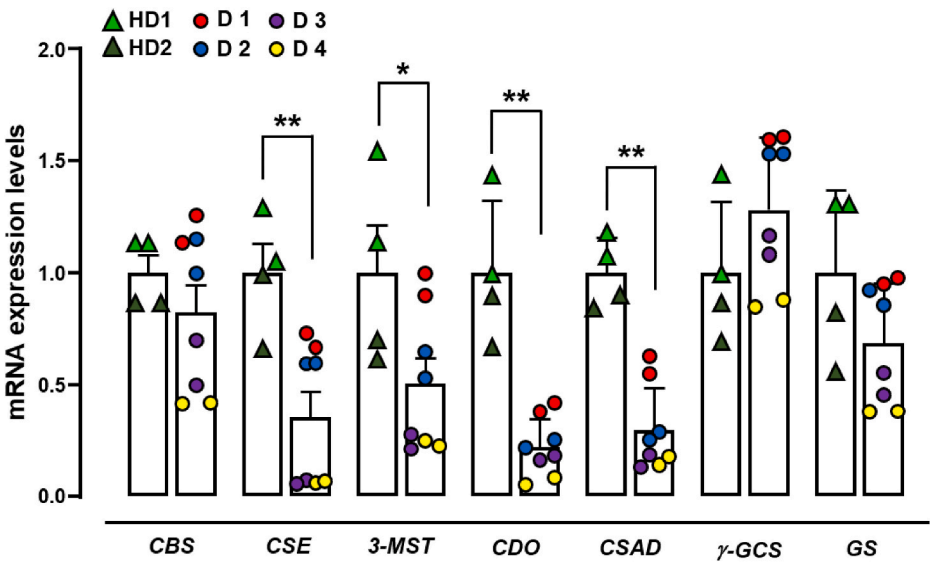

Fig. 2. mRNA expression levels of TSP genes in human primary myoblasts isolated from DMD donors. Bar graphs showing the CBS, CSE, 3-MST, CDO, CSAD, γ-GCS and GS mRNA expression levels in primary human myoblasts isolated from two healthy (HD1 and HD2) and four DMD donors (D1–D4). The quantification of transcripts has been performed in duplicate for each donor as indicated by the single dots shown on the graph. The difference in the expression levels of TSP genes are calculated by combining healthy and/or DMD donors together. Each bar is, therefore, the mean ± SEM of two healthy vs four DMD donors. *$p \leq 0.05$ and **$p \leq 0.01$ vs healthy donors.

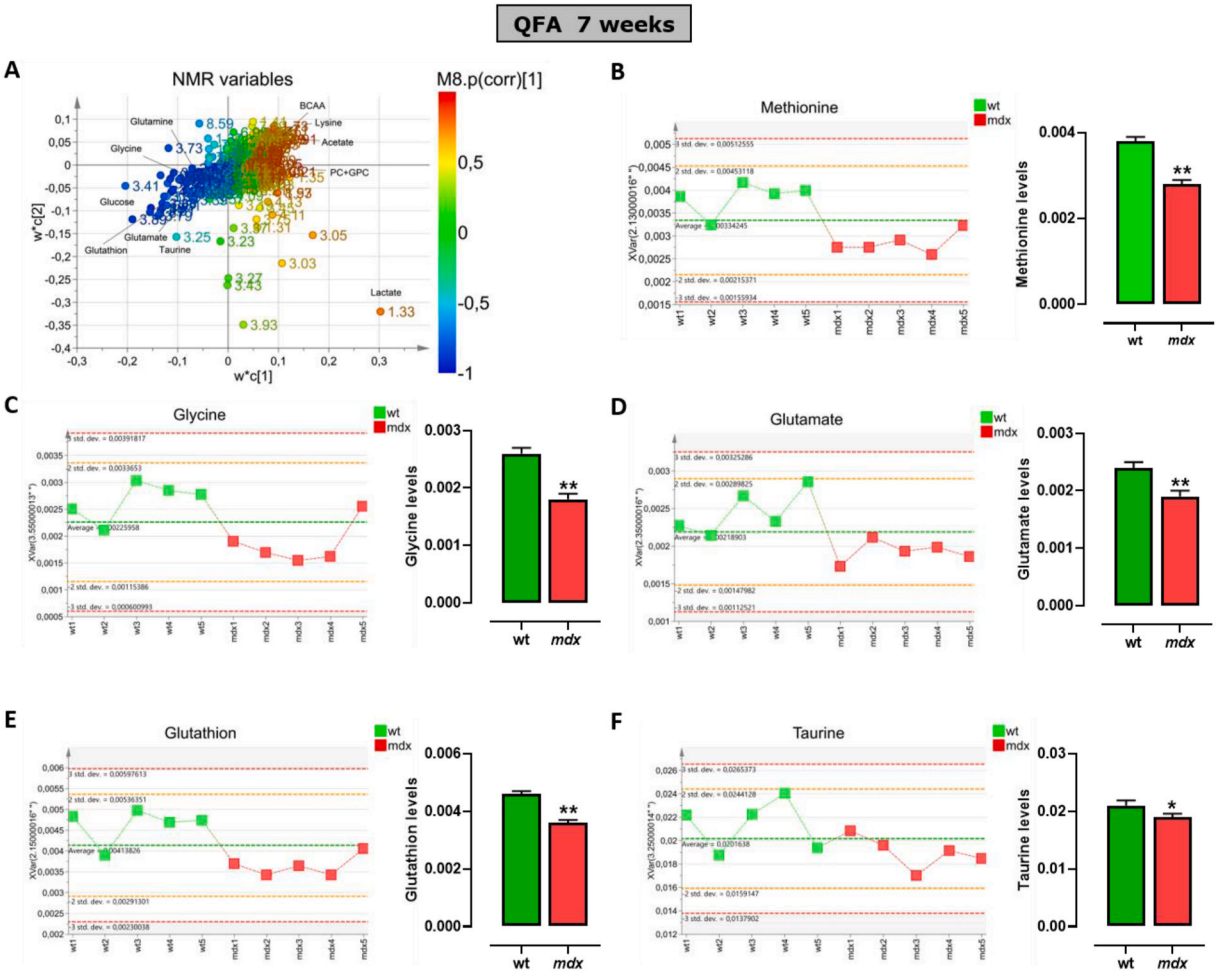

Fig. 3. Levels of main metabolites regulating the transsulfuration pathway in skeletal muscles of 7 weeks old control and *mdx* mice measured by NMR. (A) Scatter plots displaying the metabolite distribution of all classes of metabolites identified in quadriceps femoris muscle of control and *mdx* mice. (B–F) Left, graphs showing the levels of methionine, glycine, glutamate, glutathione and taurine detected in each control wild type (wt) (n = 5) or dystrophic mouse (n = 6). Right, the bar graphs show the mean values ± SEM per group. Differences are considered statistically significant when p was ≤0.05. Single asterisk (*) or double asterisk (**) denote a p-value of ≤0.05 and 0.01 vs wt mice.

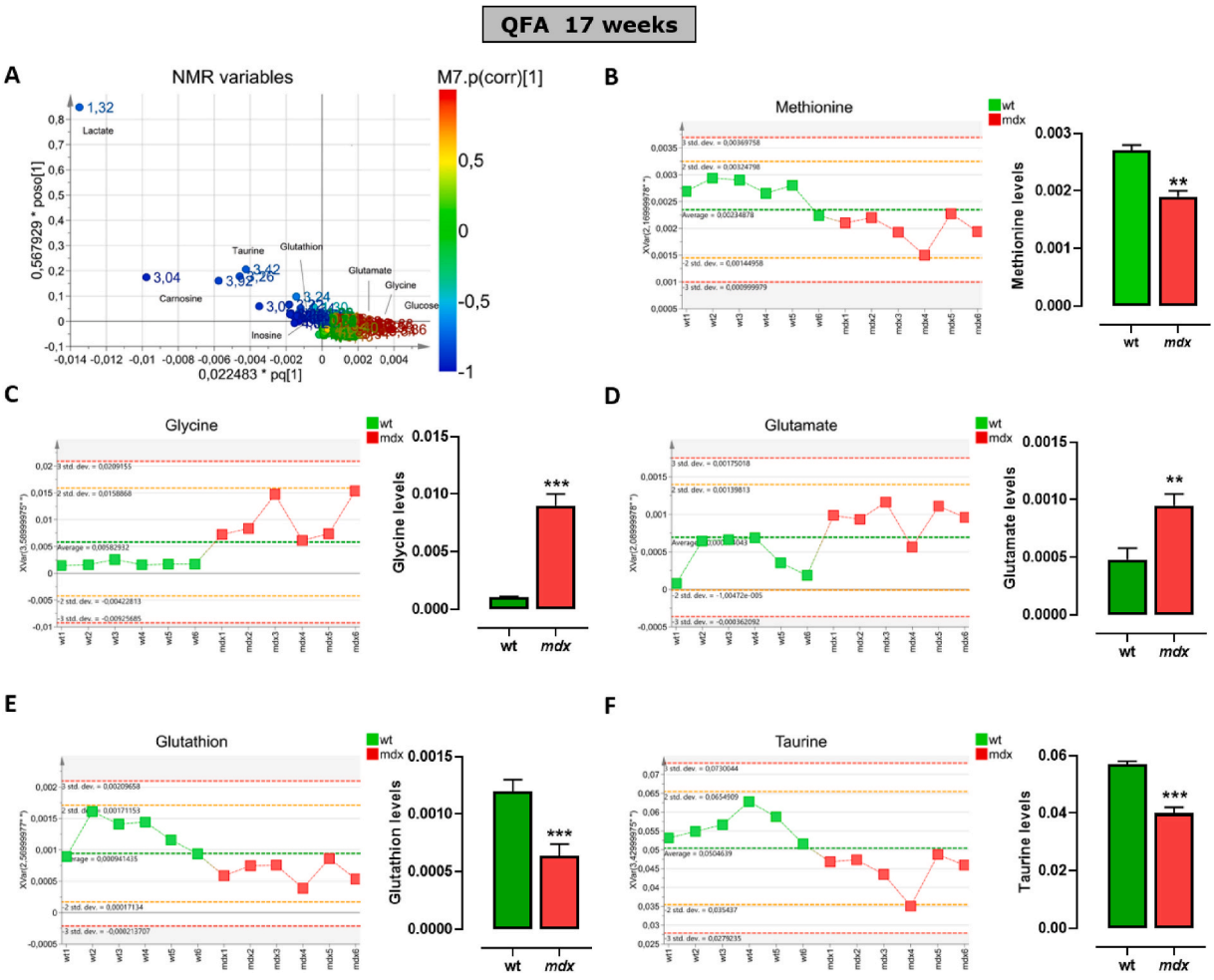

Fig. 4. Levels of main metabolites regulating the transsulfuration pathway in skeletal muscles of 17 weeks old control and *mdx* mice measured by NMR. (A) Scatter plots displaying the metabolite distribution of all classes of metabolites identified in quadriceps femoris muscle of control and *mdx* mice. (B–F) Left, graphs showing the levels of methionine, glycine, glutamate, glutathione and taurine detected in each control wt (n = 6) or dystrophic mouse (n = 6). Right, the bar graphs show the mean values ± SEM per group. Differences are considered statistically significant when *p* was ≤0.05. Double asterisk (**) and triple asterisk (***) denote a *p*-value of ≤0.01 and 0.001 vs wt mice.

to control mice (Fig. 4C and D). Methionine, GSH and L-taurine levels instead remain significantly lower (Fig. 4A, E and F). Unfortunately, the measurement of L-cysteine and hypotaurine was not successful due to technical issues caused by detection and quantification limits. This because often with complex mixtures, as for metabolic profiles, the signal arising for metabolites with a concentration lower than one order of magnitude (as L-cysteine versus taurine) appears proportionally flattened and hardly distinguishable from the background noise. Similar results have been obtained in the gastrocnemius muscle (Fig. S2 and S3).

To confirm the impairment of the H_2S pathway in dystrophic muscles, endogenous levels of H_2S have been measured in QFA of both control and *mdx* mice, by using the methylene blue assay. This colorimetric assay, widely used in biological samples, measures the H_2S content in basal condition and following L-cysteine challenge, being L-cysteine the key substrate of H_2S-generating enzymes. As shown in figure S4, no difference in H_2S levels has been detected between wt and *mdx* mice at 7 weeks of age, neither in basal nor following L-cysteine addition. The significant increase of H_2S content following L-cysteine addition (reported in figure S4 with ***) ensures the proper enzymes activity (Fig. S4A). At 17 weeks of age instead, the H_2S content was significantly lower in *mdx* mice compared to their controls in both basal and L-cysteine-stimulated conditions of almost 50% and 30%, respectively (Fig. S4B) confirming the impairment of H_2S biosynthesis in dystrophic muscle.

2.3. Expression levels of TSP genes are impaired in SKM of mdx mice

To gain further information about TSP and H_2S in DMD muscles, we measure the expression levels of CBS, CSE, 3-MST, CDO, CSAD, γ-GCS and GS genes in QFA and gastrocnemius of control and *mdx* mice at both 7 and 17 weeks using quantitative-PCR (qPCR) analysis. As shown in Fig. 5A and B, in *mdx* mice the expression of CSE, 3-MST, CDO, CSAD, γ-GCS and GS (but not CBS) is robustly reduced compared to healthy mice. Notably, the reduced expression of all the genes, also including CBS, is even more pronounced between *mdx* and control mice at 17 weeks of age (Fig. 5C and D). In summary, the results so far show that the expression of key genes and metabolites regulating the TSP pathway is dysregulated in *mdx* mice from the early stages of the disease, to undergo even greater modifications along with the disease progression.

2.4. Sodium hydrosulfide (NaHS) treatment recovers locomotor activity and ameliorates the inflammatory/fibrotic status of mdx mice

To assess if the TSP impairment and, more specifically, the reduced H_2S-generating enzymes expression could contribute to DMD-related locomotor activity impairment, *mdx* mice have been treated orally with H_2S-donor i.e. NaHS and the muscle strength has been evaluated using two different locomotor activity tests i.e. rotarod and weight test (*28*). In details, at 5 weeks of age, dystrophic mice have received 3 mg

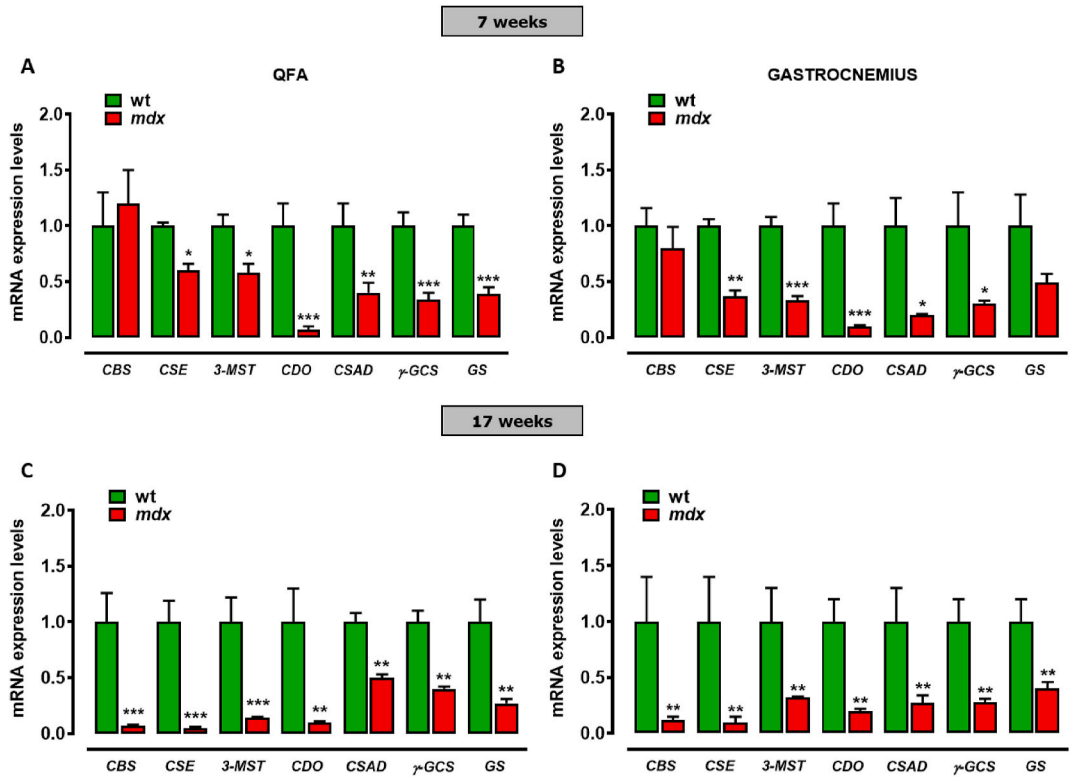

Fig. 5. mRNA expression levels of TSP genes in skeletal muscles of *mdx* mice. Bar graphs showing the quantification of transcripts levels of CBS, CSE, 3-MST, CDO, CSAD, γ-GCS and GS evaluated by qPCR in QFA and gastrocnemius of control wt (n = 6) and *mdx* mice (n = 6). Control and *mdx* mice have been compared at both 7 (A–B) and 17 (C–D) weeks. Data are expressed as $2^{-\Delta\Delta ct}$ relative to ribosomal protein S16, as described in materials and methods. Differences are considered statistically significant when p was ≤0.05. Single asterisk (*), double-asterisk (**) and triple asterisk (***) denote a p-value of ≤0.05, 0.01 and 0.001 vs wt mice.

kg^{-1} of NaHS up to 7 weeks (short treatment) or up to 17 weeks (prolonged treatment). As shown in Fig. 6A and B, both short (2 weeks) and prolonged treatment (12 weeks) with NaHS fully recover the locomotor activity when compared to the vehicle, at the same extent observed for healthy mice. To verify whether the recovery of locomotor activity of *mdx* mice by NaHS was coupled to an improvement of skeletal muscle structure, histological analysis has been performed. As shown in Fig. 6D, in QFA of *mdx* mice, the H&E, as well as the trichrome staining shows the classical hallmarks of the pathology: disorganized tissue architecture, cell infiltration and large necrotic areas (Fig. 6D and G) compared to healthy mice (Fig. 6C and F). NaHS treatment reduces the area of both necrosis and infiltrated cells, as well as fibrosis (Fig. 6E and H).

2.5. NaHS treatment positively affects inflammatory and autophagy markers in mdx mice

It is known that muscle inflammation, fibrosis and defective autophagy are patho-physiological events exacerbating DMD severity [7–9]. To verify the potential beneficial effect of H_2S donor treatment on these processes, mRNA levels of key genes regulating inflammation, fibrosis and autophagy have been analyzed.

At 7 weeks of age, QFA of dystrophic mice displays a significant increase in the expression of tumour necrosis factors-α (*TNFα*), interleukin 6 (*IL-6*), interleukin 1β (*IL-1*β), Transforming Growth Factor β (*TGF-β*) (Fig. 7A–D) in comparison to healthy tissues. In these mice, NaHS treatment prevents the increased expression of these genes. Notably, at 17 weeks of age, *mdx* mice display a different pattern of expression, with a mild reduction of pro-inflammatory markers expression, coupled to a further increase of the fibrotic marker *TGF-β*, not only versus the group of the same age treated with the vehicle, but also vs 7 weeks old *mdx* mice (Fig. 7E–H). These results suggest that at this stage of the pathology compensative mechanisms could take place to resolve skeletal muscle inflammation, even though they fail to halt the fibrosis development. Noteworthy, treatment of *mdx* mice with NaHS prevents the up-regulation of both pro-inflammatory genes and *TGF-β* (Fig. 7A–H). Analogue beneficial effects have been found in gastrocnemius (Fig. S5). Muscle autophagy has been also measured by PCR array in both *mdx* and control mice. As shown in Fig. 8A, transcriptomic analysis reveals a significant reduction in the expression of key genes regulating autophagy, including Lamp1, Becn1, PiK3c3, Atg3, Atg4, Atg7 and Ulk1, in *mdx* compared to control mice. Following 2 weeks of treatment (7 weeks of age) NaHS treatment partially but significantly recovers the expression of the aforementioned genes (Fig. 8A). These results have been validated by single PCR analysis (Fig. 8B–E) in which the data obtained by the array have been confirmed. In addition, evaluation of pAKT/AKT ratio by Western blot analysis has been performed on QFA, to measure potential changes in the AKT activation, a master negative regulator of autophagy [7, 29]. As shown in Fig. 8F, in agreement with previous studies [30, 31], a significant increase in the pAKT/AKT ratio between control and *mdx* mice have been detected. Treatment with NaHS prevents the increased phosphorylation of AKT (Fig. 8F). To further clarify the mechanism through which H_2S produced beneficial effects in *mdx* mice, the expression of LC3 (microtubule-associated protein 1 light chain 3) protein, a canonical marker of autophagy, has been measured. It is known that LC3 exists in two forms LC3-I and LC3-II. In particular, the conversion of LC3I to LC3II is a cellular event required for autophagosome formation and activity [32]. In DMD muscles, this process is compromised causing an accumulation of LC3I due to autophagy *impasse*. As shown in Fig. 8F, as expected, we have found a significant decrease of LC3-II expression in QFA of *mdx* compared to control mice. Importantly, the treatment with NaHS up to 7 weeks rescued LC3-II expression in muscles of *mdx* mice (Fig. 8G–I).

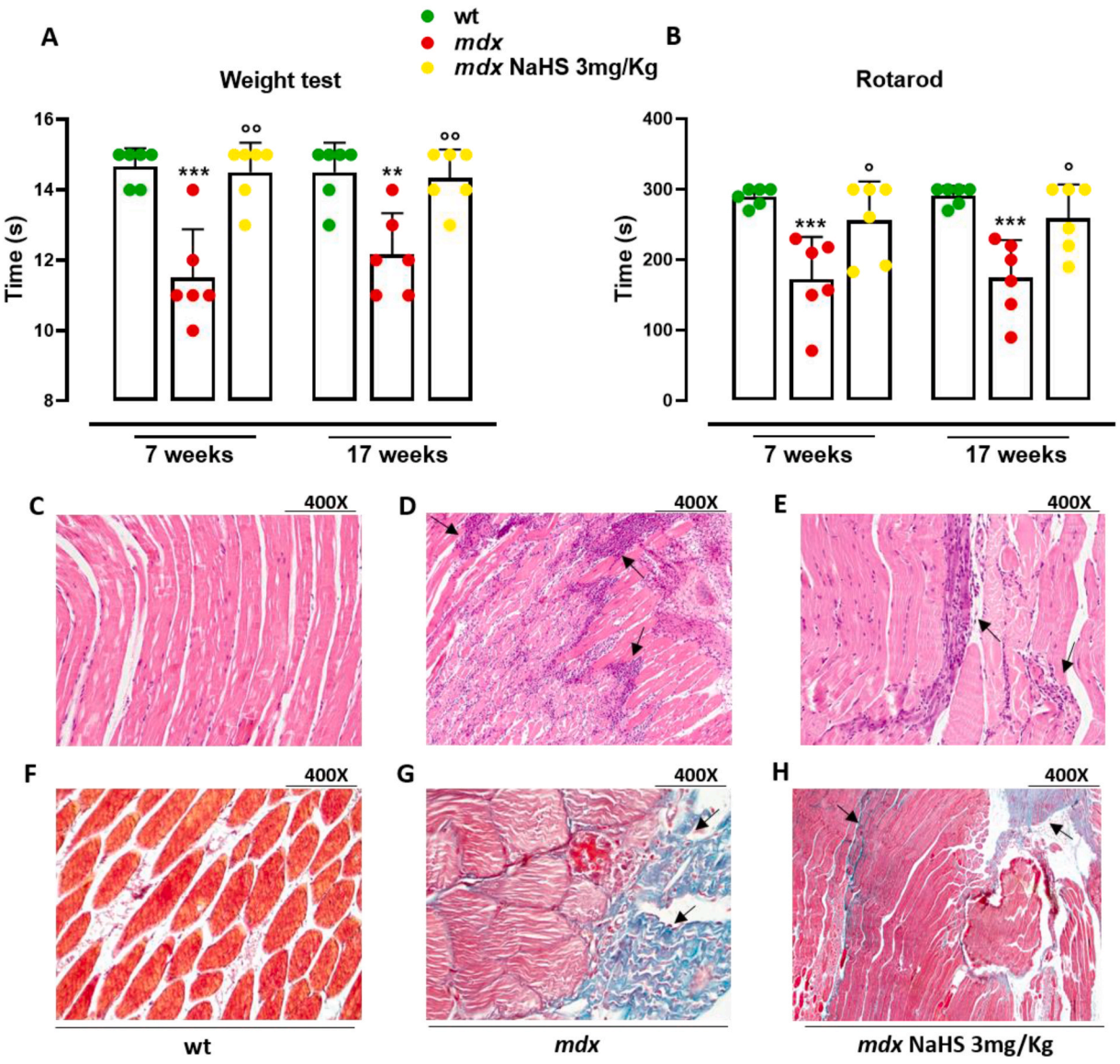

Fig. 6. Measurement of locomotor activity and histological analysis in control and *mdx* mice treated with NaHS. Muscle coordination and strength were evaluated by the weight (A) and rotarod (B) tests, measured in wt (n = 6) and *mdx* (n = 6) mice treated with vehicle or NaHS (3 mg kg^{-1}). Wt and *mdx* mice were daily treated (for two weeks), starting from week 5 to week 7 or up to week 17. Differences are considered statistically significant when *p* was ≤0.05. Double asterisk (**) and triple asterisk (***) denote a p-value of ≤0.05, 0.01 and 0.001 vs wt mice. Single circle (°) and double circle (°°) denote a *p*-value of ≤0.05 and 0.01 vs *mdx* mice of the same age. Histological analysis (C–H) has been performed on QFA of wt and *mdx* mice treated with vehicle or NaHS at 7 weeks (400× magnification). Typical histological hallmarks of dystrophic muscle (disorganized tissue architecture, cell infiltrates and fibrotic area) are highlighted in *mdx* mice by using H&E staining (D) and Goldner's trichrome staining (G). NaHS exerts a beneficial action on the amount of both cell infiltrate (see black arrow in panels D and E) and fibrotic area (see black arrow in G and H).

3. Discussion

Nowadays, an effective cure for Duchenne muscular dystrophy is still not available despite many experimental therapeutic approaches including read-through therapy, exon skipping, vector-mediated gene therapy, cell therapy, which have been tested in preclinical and clinical studies. These include also innovative strategies such as CRISPR/Cas9 genome editing and stem cell-based therapies. Unfortunately, the low efficiency in targeting skeletal muscle, low stability and host immune response have hampered the success of this therapeutic approach [33–36]. Therefore, palliative experimental therapies aimed to limit inflammation, fibrosis and necrosis by regulating intracellular targets including nuclear hormone receptors, NADPH-oxidases, Ca^{2+} channels, nuclear factor-κB (NFκB), TGF-β/myostatin production or action that, to date, remains the unique therapeutic possibility to counteract the complex pathogenesis of DMD [37, 38].

Dystrophin deficiency is tightly linked to oxidative stress in SKM. Several experimental studies report some beneficial effects of anti-oxidant therapies on dystrophy progression [39–41]. However, clinical trials evaluating the efficacy of antioxidants in DMD patients have been failed to produce the expected outcome, most likely due to the lack of our knowledge on the specific nature of the oxidative stress involved in muscular dystrophy.

It is known that H_2S is a powerful antioxidant endogenous molecule that not only inhibits reactive oxygen species (ROS) production but also neutralizes them by direct scavenging [42–45]. H_2S displays also an indirect antioxidant activity through the up-regulation of GSH, as well as, an increased expression of antioxidant enzymes [45–50]. Anti-inflammatory and cytoprotective properties of H_2S are also well documented [51]: inhibition of NFκB pathway by H_2S has been reported

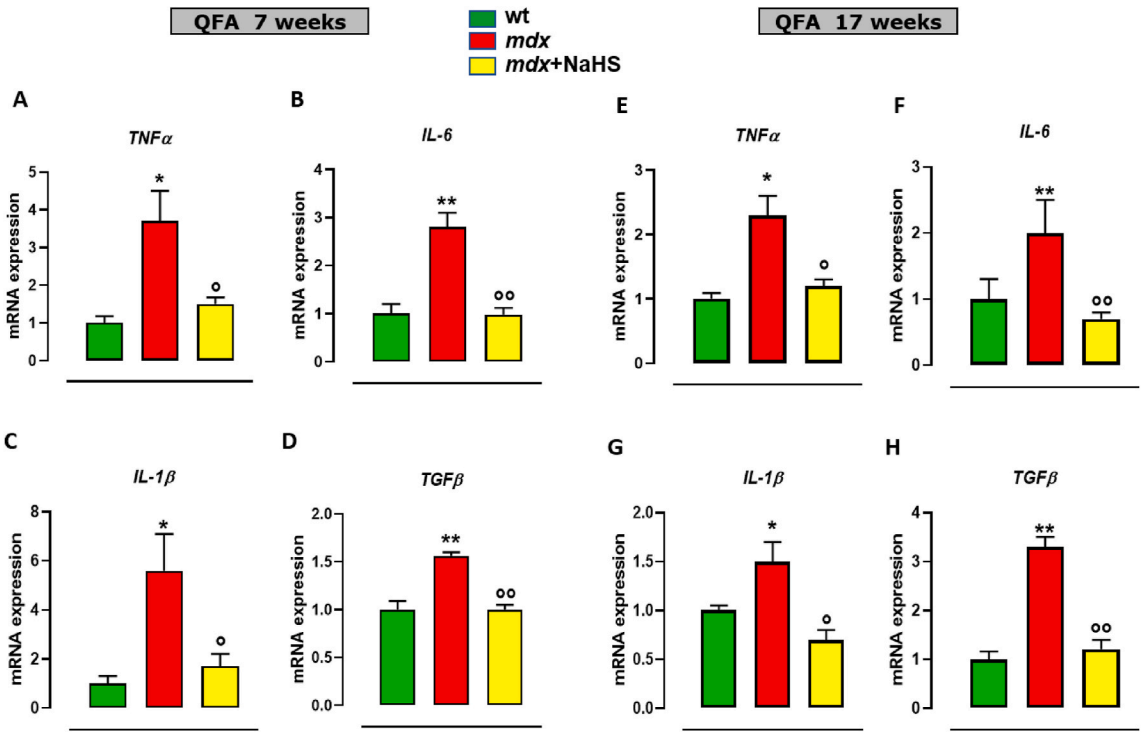

Fig. 7. mRNA expression levels of inflammation markers in skeletal muscles of *mdx* mice treated with NaHS. Bar graphs showing the mRNA expression levels of tumour necrosis factor-alpha (TNFα), interleukin 6 (IL-6), interleukin 1β (IL-1β) and transforming growth factor-beta (TGF-β) in quadriceps femoris of control and *mdx* mice receiving or not NaHS of both 7 (A–D) and 17 (E–D) weeks. Data are expressed as $2^{\wedge\text{-}\Delta\Delta ct}$ relative to ribosomal protein S16, as described in materials and methods. Single asterisk (*) and double asterisk (**) denote a *p*-value of ≤0.05 and 0.01 vs wt mice of the same age. Single circle (°) and double circle (°°) denote a *p*-value of ≤0.05 and 0.01 vs *mdx* group of the same age.

in several animal models, and consistent with this, H_2S reduces pro-inflammatory cytokine, chemokine, and enzyme expression [52, 53]. A clinical example of the relevance of the TSP, in preserving skeletal muscle function, is furnished by hyperhomocysteinemia (HHcy). In this condition, CBS is deficient or lacking with consequent reduction of homocysteine conversion into L-cysteine. This leads to a pathological condition displaying, among its characteristic features, a functional deficit in skeletal muscle [25], [54–56] ascribed to the accrual of homocysteine rather than to a deficiency in H_2S. Starting from this evidence we hypothesize that potential alterations in H_2S metabolic pathway could contribute to the pathogenesis of DMD.

To this purpose, we have first investigated whether the expression of key genes encoding for TSP enzymes, and specifically for CBS, CSE and 3-MST, could change between human primary myoblasts isolated from healthy and DMD donors. The reduced expression of these genes in DMD patients promptly led us to investigate the role of TSP in *mdx* mice, which is considered the most used preclinical model of DMD.

Metabolomic analysis performed by NMR on two types of skeletal muscles dissected from control and *mdx* mice (i.e. quadriceps and gastrocnemius), revealed that there is a broad number of metabolites that vary in their abundance between the two mouse genotypes. Among them, we focused on five key metabolites related to TSP such as methionine, L-glycine, L-glutamate, GSH and L-taurine. Notably, we found that in the early stage of pathology all five metabolites are significantly decreased. These changes are followed at the *overt* stage (17 weeks of age) by a recovery involving L-glycine and L-glutamate, but not GSH, L-taurine and methionine. These changes are most likely due to compensatory mechanisms activated in skeletal muscles aimed at rebalancing the physiological environment. In this regard, there is evidence that both glycine and glutamate are important for activating signalling pathways that protect skeletal muscle from wasting and loss of function by reducing the oxidative and inflammatory burden. Moreover, glutamate is necessary for the glutathione synthesis pathway [57, 58]. Indeed, it is known that GSH biosynthesis requires three different amino acids: L-glycine, L-cysteine and L-glutamate. L-glycine and L-glutamate come from different biochemical pathways that do not involve the TSP (Fig. 1) [59–61] while L-cysteine mainly derives from TSP. Thus the synthesis of GSH is largely regulated by L-cysteine availability [62]. Accordingly, the derangement of TSP results in the suppression of taurine and L-cysteine levels, hence GSH content.

Similarly, to human DMD muscles, we found that the expression of all genes encoding for TSP enzymes was significantly reduced in SKM of *mdx* mice near the onset to become even more marked with the progression of the disease. These data are confirmed by the finding that H_2S content is significantly reduced in QFA of dystrophic mice. Intriguingly, indirect evidence on the role of TSP impairment in SKM function is verifiable in $CSE^{-/-}$ mice generated by Ishii et al. [63], as an animal model of cystathioninemia/cystathioninuria. In particular, mice fed from 3 weeks with a low L-cysteine diet develop an acute myopathy associated with a reduced level of glutathione in SKM and the liver. Indeed, $CSE^{-/-}$ mice display a progressive paralysis of lower extremities and severe atrophy in the abdominal regions, the trapezius and rectus femoris muscles. Thereafter, the mice become lame, paralysed in the upper extremities, and eventually die.

Therefore, to understand whether and how the TSP dysregulation, and specifically of H_2S impairment occurring in DMD and *mdx* murine muscle, contribute to the severity and progression of the disease, we treated *mdx* mice with the H_2S-donor (NaHS) for a short (2 weeks) and prolonged time (12 weeks). Importantly, we found that both short or prolonged treatment with NaHS fully prevented the loss of locomotor activity in *mdx* mice. Histological analysis performed on QFA of *mdx* mice, reveals that NaHS treatment reduces the area of both necrosis and infiltrated cells, as well as fibrosis, typical hallmarks of the dystrophic tissue.

Our biochemical analyses revealed that the beneficial NaHS effect observed *in vivo* was attributable to the reduced inflammation and

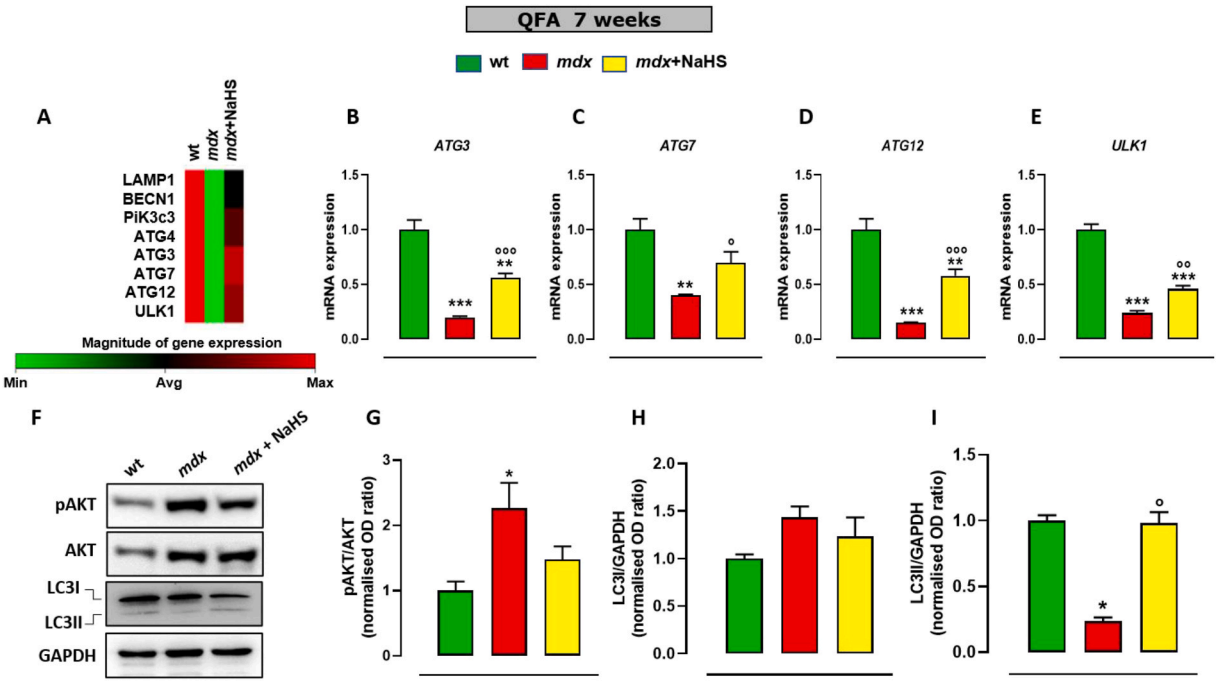

Fig. 8. mRNA expression levels of autophagy markers in skeletal muscles of *mdx* mice treated with NaHS. (A) Heatmap representation of selected genes obtained from PCR array analysis performed in QFA muscles isolated from 7-week-old control (n = 6) and *mdx* mice treated with vehicle (n = 6) or NaHS (n = 6). Red, physiological gene expression; green, gene downregulation. (B–E) Bar graphs showing the mRNA expression levels of Atg3, Atg7, Atg12 and Ulk1 in quadriceps femoris of 7 weeks old control and *mdx* mice receiving or not NaHS. Data are expressed as $2^{-\Delta\Delta ct}$ relative to actin, as described in materials and methods. (F–I) Western blot analysis showing the changes in the expression and/or phosphorylation of the two markers of autophagy/apoptosis AKT and LC3 in QFA of control and *mdx* mice treated or not with NaHS. Fold data represent the mean ± SEM of three separate experiments. The blots shown are representative of three independent experiments with similar outcomes. The GAPDH bands confirm that similar amounts of proteins were loaded on the gel for each sample. Single asterisk (*), double asterisk (**) and triple asterisk (***) denote a *p*-value of ≤0.05, 0.01, 0.001 vs wt mice, respectively. Single circle (°), double circle (°°) and triple circle (°°°) denote a *p*-value of ≤0.05, 0.01, 0.001 vs *mdx* group, respectively. (For interpretation of the references to color in this figure legend, the reader is referred to the Web version of this article.)

restoration of autophagy in skeletal muscle tissues. In particular, the high levels of both pro-inflammatory cytokines IL-1β, IL-6, TNFα, and the growth factor TGFβ measured in skeletal muscle of *mdx* mice, are lowered to physiological levels following NaHS treatment. Besides, the reduced expression of key genes regulating autophagy observed between skeletal muscles of control and *mdx* was fully prevented by NaHS, indicating the reactivation or potentiation of regenerative processes promoted by the drug. Whilst the data collected in the *overt* stage

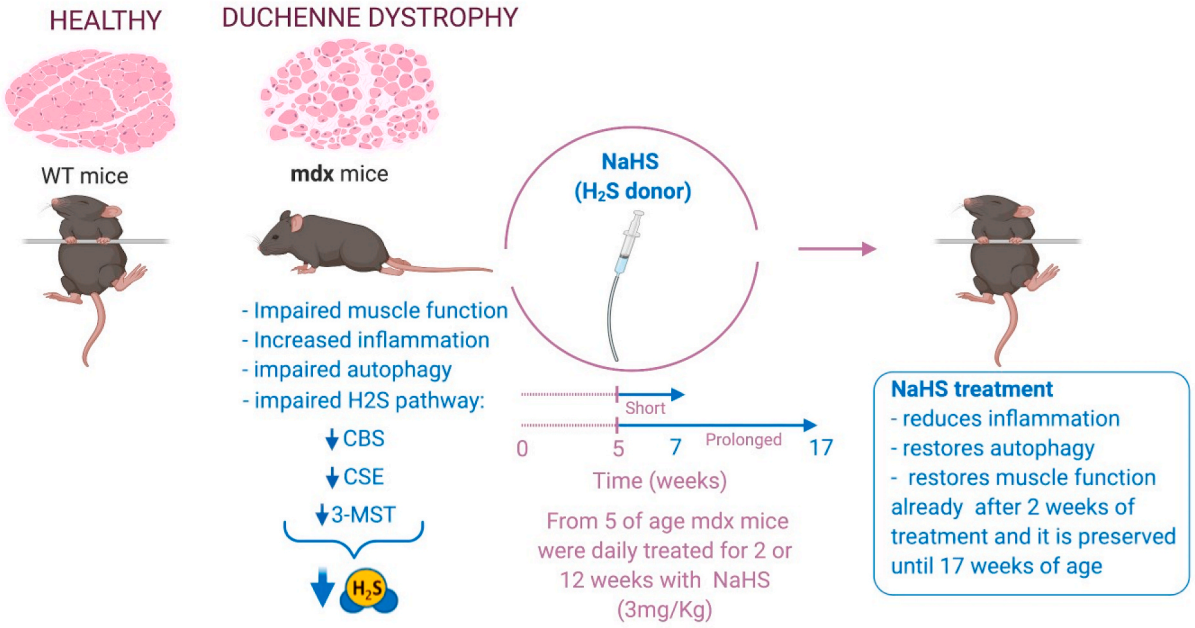

Fig. 9. Graphical abstract.

confirm the protective effect of H_2S that is mainly due to the halting of inflammation rather than the restoration of autophagy. Most likely, at this stage, with the aggravation of the pathology, the H_2S replenishment is not enough to recover autophagy. Further studies are indeed required to evaluate this hypothesis.

In conclusion, our study has revealed an important role of H_2S metabolism in the pathogenesis of DMD. The two major findings are: i) derangement of TSP can be considered a novel hallmark of DMD since in both murine and human DMD the expression of main enzymes of the TSP is markedly reduced; ii) the exogenous replacement of H_2S with NaHS significantly ameliorates the molecular features of DMD (inflammation, fibrosis and autophagy), translating *in vivo* in the complete restoration of muscular strength (Fig. 9).

This evidence could unveil a possible new alternative/additive approach in the complex managing of DMD therapy, that still relies on high doses of glucocorticoids, with all the negative consequences associated.

4. Materials and methods

4.1. Animal care and use

The experimental protocol was evaluated and approved by the Institutional Animal Ethics Committee for the use of experimental animals and conformed to guidelines for the safe use and care of experimental animals under the Italian D.L.no. 116 of 27 January 1992; Ministero Della Salute Authorization n. 961-2018-PR and associated guidelines in the European Communities Council (86/609/ECC and 2010/63/UE). For this study, male wild-type (C57BL/10ScSnJ) and *mdx* (C57BL/10ScSn-DMD*mdx*/J) mice of 5 weeks of age weighing approximately 20–25 g were purchased from Charles River Laboratories (MI, Italy). All mice were housed in an individually ventilated cage system with a 12 h light-dark cycle (temperature 23 ± 2 °C, humidity 60%) and received standard mouse chow (Harlan Teklad) and water *ab libitum*. NaHS (3 mg kg^{-1}) or vehicle (potassium phosphate buffer pH 7.4) was administered orally to mice once a day for two weeks (from 5 to 7 weeks) and from 5 to 17 weeks. Animals were housed in groups of five to six; animals belonging to each cage were randomly assigned to the different experimental groups. The experimenter performing the behavioural testing was blind to the genotype and treatment.

4.2. Locomotor tests

The rotarxod and weight tests were performed in control and dystrophic mice immediately before the beginning of the pharmacological treatment (5 weeks) and at the end (7 or 17 weeks) of treatment with vehicle, or NaHS following published procedures (*9*). In our rotarod protocol, the latency to fall was changed over a maximum period of 300 s.

4.3. Nuclear Magnetic Resonance (NMR)

To extract metabolites of interest (e.g., lipids, amino acids, carbohydrates and other small metabolites), while leaving other compounds (e.g., DNA, RNA and proteins) in tissue pellet, tissues were mechanically disrupted. Combined extraction of polar and lipophilic metabolites was carried out by using methanol/water/chloroform as suggested by the Standard Metabolic Reporting Structures working group [64]. Homogenization of 14 mg of frozen muscle tissue was carried out in 480 μl of methanol and 106 μl of water (all solvents were cold) with UltraTurrax for 2 min on ice. Then 240 μl of chloroform was added and the mixture was vortexed for 30 s. The homogenate was gently stirred and mixed, on ice, for 10 min and then another 240 μl of water and 240 μl of chloroform were added and the final mixture was vortexed and centrifuged at 10000 rpm for 15 min at 4 °C. This procedure separates three phases: water/methanol at the top (polar fraction, containing polar metabolites), denatured proteins and cellular debris in the middle, and chloroform at the bottom (nonpolar fraction, containing lipophilic metabolites). Polar and nonpolar fractions were transferred into glass vials and the solvents removed by using a rotary vacuum evaporator at room temperature and stored at −80 °C until they were analyzed.

4.4. NMR measurements of polar metabolites

For NMR analysis, polar fractions were resuspended in 630 μl of phosphate buffer saline (PBS, pH 7.4), adding 70 μl of ^2H_2O solution [containing 1 mM sodium 3-trimethylsilyl [2,2,3,3-$^2H_4$] propionate (TSP) as a chemical shift reference for ^1H spectra] to provide a field frequency lock, reaching 700 μl of total volume. The nonpolar fractions instead, were resuspended in 700 μl of C^2HCl_3. The samples were then transferred in NMR tubes for analysis. One-dimensional (1D) spectra were acquired at 600.13 MHz on a Bruker Avance III-600 spectrometer equipped with a TCI CryoProbeTM fitted with a gradient along the Z-axis, at a probe temperature of 27 °C, using the excitation sculpting sequence for solvent suppression [65]. Spectra were referred to internal 0.1 mM sodium trimethylsilyl propionate (TSP), assumed to resonate at $\delta = 0.00$ ppm. These spectra were used for multivariate statistical analysis. In addition, two-dimensional (2D) clean total-correlation spectroscopy (TOCSY) and heteronuclear single quantum coherence (HSQC) experiments were acquired to help metabolite identification and signals assignment. 2D spectra were referenced to the lactate doublet assumed to resonate at $\delta = 1.33$ ppm for ^1H, and $\delta = 20.76$ ppm for ^{13}C.

4.5. NMR data processing and multivariate statistical analysis

For muscle datasets (gastrocnemius and anterior femoral quadriceps) collected from mice at different age (7 weeks and 17 weeks), selected spectral area were defined: 0.50–9.50 ppm (7 weeks and 17 weeks gastrocnemius), 0.50–9.50 ppm (7 weeks anterior femoral quadriceps), and 0.70–9.40 ppm (17 weeks anterior femoral quadriceps). Each proton spectrum was automatically segmented into integrated regions (buckets) of 0.02-ppm each using the AMIX 3.6 package (Bruker Biospin, Germany). The residual water resonance region (4.60–5.10 ppm) was excluded, and the binned regions were normalized to the total spectrum area. Multivariate statistical data analysis was applied to each dataset to differentiate *mdx* and the healthy muscles profiles through NMR spectra, according to their different metabolic content. Each integrated dataset was reshaped as a matrix and imported into SIMCA-P+ 15 package (Umetrics, Umea, Sweden) where unsupervised PCA, supervised PLS-DA and OPLS-DA discriminant analyses were performed. PCA was first applied to check outliers and uncover initial trends within the dataset by investigating the systematic variation in the data matrix such to identify trends and clusters. Once assessed data homogeneity, PLS-DA or OPLS-DA discriminant analysis was used to improve group discrimination. Indeed, for these two approaches, data modelling is based upon multivariate regression methods which extract linear relationships from two data blocks, NMR data and class belonging, thus highlighting metabolic changes responsible for specific alteration in *mdx* metabolic profiles compared to the healthy animals. The performance of each elaborated model was evaluated *via* the parameters R2 and Q2, respectively indicating the goodness of fit and the goodness of prediction. Moreover, each model was validated by an internal iterative cross-validation routine with 7 rounds, permutation test response (800 repeats), and analysis of Variance (ANOVA testing of Cross-Validated predictive residuals). Selected isolated signals with $|pcorr| \geq 0.7$, VIP >1 (Variable Importance in the Projection) were then considered for univariate statistical analysis and Student's t-test.

4.6. H_2S assay

H_2S determination was performed using a methylene blue-based assay [66, 67]. Briefly, anterior femoral quadriceps collected from

mice at different age (7 weeks and 17 weeks), were homogenized in a lysis buffer (100 mM potassium phosphate buffer, pH = 7.4, sodium orthovanadate 10 mM and a cocktail of protease inhibitors 1% v/v) and the protein concentration was determined using the Bradford assay (Bio-Rad Laboratories, Milan, Italy). The lysates were added to a reaction mixture (total volume 500 μL) containing pyridoxal 5′-phosphate (2 mM, 20 μL), L-cysteine (10 mM, 20 μL) and saline (30 μL). The reaction was performed in parafilm-sealed Eppendorf tubes and initiated by transferring tubes from ice to a 37 °C water bath. After 40 min incubation, zinc acetate 1% (ZnAc; 250 μL) was added to trap any H_2S emitted followed by trichloroacetic acid 10% (TCA; 250 μL). Subsequently, N,N-dimethylphenylendiammine sulphate 20 μM (DPD; 133 μL) in 7.2 M HCl and FeCl3 (30 μM, 133 μL) in 1.2 M HCl were added. After 20 min, absorbance values were measured at a wavelength of 668 nm. All samples were assayed in duplicate, and H_2S concentration was calculated against a calibration curve of NaHS (3.12–250 μM). Results were expressed as nmol/mg protein per min.

4.7. Histological analysis

Anterior femoral quadriceps collected from wt and *mdx* treated with vehicle or NaHS at 7 weeks were fixed in neutral buffered formalin before being embedded in paraffin. Sections (4 μm) were stained with haematoxylin-eosin (H&E) or with Goldner's trichrome and analyzed under light microscopy (400× magnification). The presence and degree of degeneration/necrosis, cells inflammatory infiltration, fibrotic areas were blindly quantified according to arbitrary criteria by two independent morphologists. Blue staining represents collagen, red staining muscle tissues.

4.8. Cell culture and reagents

Primary myoblasts from healthy donors were provided by Innoprot (Bizkaia-Spain) and Sciencell (Carlsbad, CA, USA). The myoblasts were propagated in Skeletal Muscle Cell Medium (cat P60124, Innoprot, Bizkaia (Spain).

4.9. RNA extraction and quantitative PCR (qPCR)

Total RNA isolation, purification, and cDNA synthesis from murine skeletal muscle tissues were performed as described (*9*). Quantitative PCR (qPCR) was carried out in a real-time PCR system CFX96 (Bio-Rad) using the SsoAdvanced SYBR Green supermix (cat. n. 1725274, Bio-Rad Milan Italy) detection technique and specific primers are shown in Supplementary Table 1. Quantitative PCR was performed on independent biological samples ≥ 4–5 for each experimental group. Each sample was amplified simultaneously in triplicate in a one-assay run with a non-template control blank for each primer pair to control for contamination or primer-dimer formation, and the cycle threshold (Ct) value for each experimental group was determined. The housekeeping gene (actin) was used to normalize the Ct values, using the $2^{\wedge -\Delta Ct}$ formula; differences in mRNA content between groups were expressed as $2^{\wedge -\Delta\Delta Ct}$. RNA isolation and cDNA preparation from primary myoblasts from DMD donors was carried out according to previously described methods (*9*). In this case, each human cDNA was amplified simultaneously in duplicate in a one-assay run and the gene encoding for the ribosomal protein S16 was used as housekeeping.

4.10. Western blotting analysis

Before isolating the total proteins from skeletal muscles, control and/or dystrophic mice were anaesthetized with 75% CO_2/25% O_2 and sacrificed by cervical dislocation. Skeletal muscles including quadriceps were quickly removed and kept on dry ice until the whole procedure was completed. Muscles from control and *mdx* mice were homogenized in lysis buffer composed of 150 mM NaCl, 1 mM EDTA, 1% (v/v) Triton X-100, 2.5 mM sodium pyrophosphate, 1 mM 2-glycerophosphate, 1 mM Na_3VO_4, 20 mM Tris–HCl pH8.1 %SDS, plus protease inhibitor (cat. n. P8340, Sigma-Aldrich, MI Italy) at pH7.4. Lysates were kept in an orbital shaker incubator at 220 rpm at 4 °C for 30 min and then centrifuged for 15 min at 13,000 g at 4 °C. The supernatants were transferred to tubes and quantified by DC Protein Assay (Bio-Rad, Milan, Italy). Subsequently, the samples (60 μg of total protein) were heated at 70 °C for 10min in NuPAGE LDS Sample Buffer (cat. n. NP0007, Life Technology, Milan, Italy) plus Sample Reducing Agent (cat. n. NP0004, Life Technology MI Italy) and loaded on 4–12% Bis-Tris Protein Gels (cat. n. NP0336PK2, Life Technology, Milan, Italy) and then transferred to a PVDF membrane [68]. The primary antibodies used was a rabbit *p*-AKT/AKT antibody, (1:1000; cat. n. 4060); rabbit LC3B antibody (1:1000; cat. n. 2775), Cell signalling, Beverly, MA, USA). An anti–GAPDH antibody (1D4) (cat. n. NB300-221) (1:5000; Novus) was used to check for equal protein loading. Reactive bands were detected by chemiluminescence (ECL-plus; Bio-Rad, Segrate, Italy). The intensity of bands was analyzed on a ChemiDoc station with Quantity-one software (Biorad, Segrate, Italy).

4.11. Data analysis

Data were expressed as means ± SEM of values and 'n' refers to the number of samples for each set of experiments. Statistical analysis was performed using GraphPad Prism Software Inc., La Jolla, CA, USA. The Shapiro-Wilk test was used to determine if a data set was well modelled by a normal distribution or not. For samples normally distributed, the one-way analysis of variance (ANOVA) followed by Tukey's analysis was used to determine statistically significant differences between two or more independent biological groups. For samples not normally distributed we used the non-parametric Kruskal-Wallis test. Statistically significant differences were accepted when p was <0.05.

Declaration of competing interest

The authors declare no conflict of interest.

Acknowledgements

We thank Dr Elisabetta Gazzerro (Ospedale Pediatrico Gaslini - Genova) for sharing primary human cells.

Appendix A. Supplementary data

Supplementary data to this article can be found online at https://doi.org/10.1016/j.redox.2021.102040.

Funding

This work was supported by the Italian Ministry of Education, Universities and Research (MIUR) *Progetti di Rilevante Interesse Nazionale* (PRIN), grant numbers 2017XZMBYX. FAI received a research grant by Duchenne Parent Project DL.

Author contributions

V.V., E.P., O.L.M. and M.S. performed the locomotor tests and analyzed the data. F.A.I. performed cell culture, Western blot experiments and analyzed the data. E.P. and M.S. performed RT-PCR experiments and analyzed the data. D.P. performed the NMR experiments and analyzed the data. N.M., A.B. and G.d.D. perform histological experiments. M.B., V.V., E.P. and F.A.I. conceived and designed the study, M.B. and G.C. coordinated all the data. M.B., E.P. and V.V. wrote the manuscript, A.d.L. and G.C. revised the manuscript.

References

[1] A.E. Stark, Determinants of the incidence of Duchenne muscular dystrophy, Ann. Transl. Med. 3 (2015), https://doi.org/10.3978/j.issn.2305-5839.2015.10.45.

[2] B.J. Petrof, J.B. Shrager, H.H. Stedman, A.M. Kelly, H.L. Sweeney, Dystrophin protects the sarcolemma from stresses developed during muscle contraction, Proc. Natl. Acad. Sci. Unit. States Am. 90 (1993) 3710–3714.

[3] J. Ehmsen, E. Poon, K. Davies, The dystrophin-associated protein complex, J. Cell Sci. 115 (2002) 2801–2803.

[4] A. Sacco, F. Mourkioti, R. Tran, J. Choi, M. Llewellyn, P. Kraft, M. Shkreli, S. Delp, J.H. Pomerantz, S.E. Artandi, H.M. Blau, Short telomeres and stem cell exhaustion model Duchenne muscular dystrophy in mdx/mTR mice, Cell 143 (2010) 1059–1071.

[5] S. Miyatake, Y. Shimizu-Motohashi, S. Takeda, Y. Aoki, Anti-inflammatory drugs for Duchenne muscular dystrophy: focus on skeletal muscle-releasing factors, Drug Des. Dev. Ther. 10 (2016) 2745–2758.

[6] Y. Nitahara-Kasahara, S. Takeda, T. Okada, Inflammatory predisposition predicts disease phenotypes in muscular dystrophy, Inflamm. Regen. 36 (2016) 14.

[7] M. Sandri, L. Coletto, P. Grumati, P. Bonaldo, Misregulation of autophagy and protein degradation systems in myopathies and muscular dystrophies, J. Cell Sci. 126 (2013) 5325–5333.

[8] C. De Palma, F. Morisi, S. Cheli, S. Pambianco, V. Cappello, M. Vezzoli, P. Rovere-Querini, M. Moggio, M. Ripolone, M. Francolini, M. Sandri, E. Clementi, Autophagy as a new therapeutic target in Duchenne muscular dystrophy, Cell Death Dis. 5 (2014) e1363.

[9] F.A. Iannotti, E. Pagano, A.S. Moriello, F.G. Alvino, N.C. Sorrentino, L. D'Orsi, E. Gazzerro, R. Capasso, E. De Leonibus, L. De Petrocellis, V. Di Marzo, Effects of non-euphoric plant cannabinoids on muscle quality and performance of dystrophic mdx mice, Br. J. Pharmacol. 176 (2019) 1568–1584.

[10] J.I. Sbodio, S.H. Snyder, B.D. Paul, Regulators of the transsulfuration pathway, Br. J. Pharmacol. 176 (2019) 583–593.

[11] Y. Wang, R. Yu, L. Wu, G. Yang, Hydrogen sulfide signaling in regulation of cell behaviors, Nitric Oxide 103 (2020) 9–19.

[12] C. Szabó, Hydrogen sulphide and its therapeutic potential, Nat. Rev. Drug Discov. 6 (2007) 917–935.

[13] O. Kabil, R. Banerjee, Redox biochemistry of hydrogen sulfide, J. Biol. Chem. 285 (2010) 21903–21907.

[14] C.R. Powell, K.M. Dillon, J.B. Matson, A review of hydrogen sulfide (H2S) donors: chemistry and potential therapeutic applications, Biochem. Pharmacol. 149 (2018) 110–123.

[15] F. Sun, J.-H. Luo, T.-T. Yue, F.-X. Wang, C.-L. Yang, S. Zhang, X.-Q. Wang, C.-Y. Wang, The role of hydrogen sulfide signaling in macrophage activation, Immunology (2020), https://doi.org/10.1111/imm.13253.

[16] P. Nagy, G. Schwarz, S. Kopriva, Highlighted mechanistic aspects in the chemical biology of reactive sulfur species, Br. J. Pharmacol. 176 (2019) 511–513.

[17] N. Dilek, A. Papapetropoulos, T. Toliver-Kinsky, C. Szabo, Hydrogen sulfide: an endogenous regulator of the immune system, Pharmacol. Res. 161 (2020) 105119.

[18] G.J. McBean, M. Aslan, H.R. Griffiths, R.C. Torrão, Thiol redox homeostasis in neurodegenerative disease, Redox Biol 5 (2015) 186–194.

[19] B.D. Paul, J.I. Sbodio, S.H. Snyder, Cysteine metabolism in neuronal redox homeostasis, Trends Pharmacol. Sci. 39 (2018) 513–524.

[20] S. Schaffer, H.W. Kim, Effects and mechanisms of taurine as a therapeutic agent, Biomol Ther (Seoul). 26 (2018) 225–241.

[21] I. Bellezza, F. Riuzzi, S. Chiappalupi, C. Arcuri, I. Giambanco, G. Sorci, R. Donato, Reductive stress in striated muscle cells, Cell. Mol. Life Sci. 77 (2020) 3547–3565.

[22] S. Li, R. Liao, X. Sheng, X. Luo, X. Zhang, X. Wen, J. Zhou, K. Peng, Hydrogen gas in cancer treatment, Front Oncol 9 (2019) 696.

[23] N. Yang, Y. Liu, T. Li, Q. Tuo, Role of hydrogen sulfide in chronic diseases, DNA Cell Biol. 39 (2020) 187–196.

[24] V. Vellecco, A. Mancini, A. Ianaro, V. Calderone, C. Attanasio, A. Cantalupo, B. Andria, G. Savoia, E. Panza, A. Di Martino, G. Cirino, M. Bucci, Cystathionine β-synthase-derived hydrogen sulfide is involved in human malignant hyperthermia, Clin. Sci. 130 (2016) 35–44.

[25] V. Vellecco, A. Martelli, I.S. Bibli, M. Vallifuoco, O.L. Manzo, E. Panza, V. Citi, V. Calderone, G. de Dominicis, C. Cozzolino, E.M. Basso, M. Mariniello, I. Fleming, A. Mancini, M. Bucci, G. Cirino, Anomalous Kv7 channel activity in human malignant hyperthermia syndrome unmasks a key role for H2S and persulfidation in skeletal muscle, Br. J. Pharmacol. 177 (2020) 810–823.

[26] B.C. Lim, S. Lee, J.-Y. Shin, J.-I. Kim, H. Hwang, K.J. Kim, Y.S. Hwang, J.-S. Seo, J. H. Chae, Genetic diagnosis of Duchenne and Becker muscular dystrophy using next-generation sequencing technology: comprehensive mutational search in a single platform, J. Med. Genet. 48 (2011) 731–736.

[27] Y. Wang, Y. Yang, J. Liu, X.-C. Chen, X. Liu, C.-Z. Wang, X.-Y. He, Whole dystrophin gene analysis by next-generation sequencing: a comprehensive genetic diagnosis of Duchenne and Becker muscular dystrophy, Mol. Genet. Genom. 289 (2014) 1013–1021.

[28] M. Alame, D. Lacourt, R. Zenagui, D. Mechin, F. Danton, M. Koenig, M. Claustres, M. Cossée, Implementation of a reliable next-generation sequencing strategy for molecular diagnosis of dystrophinopathies, J. Mol. Diagn. 18 (2016) 731–740.

[29] Y.S. Gallot, K.R. Bohnert, A.R. Straughn, G. Xiong, S.M. Hindi, A. Kumar, PERK regulates skeletal muscle mass and contractile function in adult mice, Faseb. J. 33 (2019) 1946–1962.

[30] P. Spitali, P. Grumati, M. Hiller, M. Chrisam, A. Aartsma-Rus, P. Bonaldo, Autophagy is impaired in the tibialis anterior of dystrophin null mice, PLoS Curr 5 (2013), https://doi.org/10.1371/currents.md.e1226cefa851a2f079bbc406c0a21e80.

[31] C. Dogra, H. Changotra, J.E. Wergedal, A. Kumar, Regulation of phosphatidylinositol 3-kinase (PI3K)/Akt and nuclear factor-kappa B signaling pathways in dystrophin-deficient skeletal muscle in response to mechanical stretch, J. Cell. Physiol. 208 (2006) 575–585.

[32] A. Terman, B. Gustafsson, U.T. Brunk, Autophagy, organelles and ageing, J. Pathol. 211 (2007) 134–143.

[33] Y. Shimizu-Motohashi, S. Miyatake, H. Komaki, S. Takeda, Y. Aoki, Recent advances in innovative therapeutic approaches for Duchenne muscular dystrophy: from discovery to clinical trials, Am J Transl Res 8 (2016) 2471–2489.

[34] Y. Shimizu-Motohashi, H. Komaki, N. Motohashi, S. Takeda, T. Yokota, Y. Aoki, Restoring dystrophin expression in Duchenne muscular dystrophy: current status of therapeutic approaches, J. Personalized Med. 9 (2019), https://doi.org/10.3390/jpm9010001.

[35] L. Echevarría, P. Aupy, A. Goyenvalle, Exon-skipping advances for Duchenne muscular dystrophy, Hum. Mol. Genet. 27 (2018) R163–R172.

[36] S. Biressi, A. Filareto, T.A. Rando, Stem Cell Therapy for Muscular Dystrophies, 2020, https://doi.org/10.1172/JCI142031.

[37] U.T. Ruegg, Pharmacological prospects in the treatment of Duchenne muscular dystrophy, Curr. Opin. Neurol. 26 (2013) 577–584.

[38] A. Salmaninejad, Y. Jafari Abarghan, S. Bozorg Qomi, H. Bayat, M. Yousefi, S. Azhdari, S. Talebi, M. Mojarrad, Common therapeutic advances for Duchenne muscular dystrophy (DMD), Int. J. Neurosci. 1–20 (2020).

[39] H.G. Radley, A. De Luca, G.S. Lynch, M.D. Grounds, Duchenne muscular dystrophy: focus on pharmaceutical and nutritional interventions, Int. J. Biochem. Cell Biol. 39 (2007) 469–477.

[40] Y.S. Hori, A. Kuno, R. Hosoda, M. Tanno, T. Miura, K. Shimamoto, Y. Horio, Resveratrol ameliorates muscular pathology in the dystrophic mdx mouse, a model for Duchenne muscular dystrophy, J. Pharmacol. Exp. Therapeut. 338 (2011) 784–794.

[41] N.P. Evans, J.A. Call, J. Bassaganya-Riera, J.L. Robertson, R.W. Grange, Green tea extract decreases muscle pathology and NF-kappaB immunostaining in regenerating muscle fibers of mdx mice, Clin. Nutr. 29 (2010) 391–398.

[42] M. Whiteman, J.S. Armstrong, S.H. Chu, S. Jia-Ling, B.-S. Wong, N.S. Cheung, B. Halliwell, P.K. Moore, The novel neuromodulator hydrogen sulfide: an endogenous peroxynitrite "scavenger"? J. Neurochem. 90 (2004) 765–768.

[43] D. Gerő, R. Torregrossa, A. Perry, A. Waters, S. Le-Trionnaire, J.L. Whatmore, M. Wood, M. Whiteman, The novel mitochondria-targeted hydrogen sulfide (H2S) donors AP123 and AP39 protect against hyperglycemic injury in microvascular endothelial cells in vitro, Pharmacol. Res. 113 (2016) 186–198.

[44] V. Citi, E. Piragine, L. Testai, M.C. Breschi, V. Calderone, A. Martelli, The role of hydrogen sulfide and H2S-donors in myocardial protection against ischemia/reperfusion injury, Curr. Med. Chem. 25 (2018) 4380–4401.

[45] Y. Kimura, H. Kimura, Hydrogen sulfide protects neurons from oxidative stress, Faseb. J. 18 (2004) 1165–1167.

[46] K. Ono, T. Akaike, T. Sawa, Y. Kumagai, D.A. Wink, D.J. Tantillo, A.J. Hobbs, P. Nagy, M. Xian, J. Lin, J.M. Fukuto, Redox chemistry and chemical biology of H2S, hydropersulfides, and derived species: implications of their possible biological activity and utility, Free Radic. Biol. Med. 77 (2014) 82–94.

[47] B.L. Predmore, D.J. Lefer, G. Gojon, Hydrogen sulfide in biochemistry and medicine, Antioxidants Redox Signal. 17 (2012) 119–140.

[48] C. Szabo, Roles of hydrogen sulfide in the pathogenesis of diabetes mellitus and its complications, Antioxidants Redox Signal. 17 (2012) 68–80.

[49] Z.-Z. Xie, Y. Liu, J.-S. Bian, Hydrogen sulfide and cellular redox homeostasis, Oxid Med Cell Longev (2016) 6043038, 2016.

[50] N. Tyagi, K.S. Moshal, U. Sen, T.P. Vacek, M. Kumar, W.M. Hughes, S. Kundu, S. C. Tyagi, H2S protects against methionine-induced oxidative stress in brain endothelial cells, Antioxidants Redox Signal. 11 (2009) 25–33.

[51] J.L. Wallace, R.W. Blackler, M.V. Chan, G.J. Da Silva, W. Elsheikh, K.L. Flannigan, I. Gamaniek, A. Manko, L. Wang, J.-P. Motta, A.G. Buret, Anti-inflammatory and cytoprotective actions of hydrogen sulfide: translation to therapeutics, Antioxidants Redox Signal. 22 (2015) 398–410.

[52] E. Ekundi-Valentim, K.T. Santos, E.A. Camargo, A. Denadai-Souza, S.A. Teixeira, C. I. Zanoni, A.D. Grant, J. Wallace, M.N. Muscará, S.K. Costa, Differing effects of exogenous and endogenous hydrogen sulphide in carrageenan-induced knee joint synovitis in the rat, Br. J. Pharmacol. 159 (2010) 1463–1474.

[53] M. Castelblanco, J. Lugrin, D. Ehirchiou, S. Nasi, I. Ishii, A. So, F. Martinon, N. Busso, Hydrogen sulfide inhibits NLRP3 inflammasome activation and reduces cytokine production both in vitro and in a mouse model of inflammation, J. Biol. Chem. 293 (2018) 2546–2557.

[54] S. Veeranki, S.C. Tyagi, Defective homocysteine metabolism: potential implications for skeletal muscle malfunction, Int. J. Mol. Sci. 14 (2013) 15074–15091.

[55] S.J. Sacharow, J.D. Picker, H.L. Levy, in: M.P. Adam, H.H. Ardinger, R.A. Pagon, S. E. Wallace, L.J. Bean, K. Stephens, A. Amemiya (Eds.), GeneReviews®, University of Washington, Seattle, Seattle (WA), 1993. http://www.ncbi.nlm.nih.gov/books/NBK1524/.

[56] A.A.M. Morris, V. Kožich, S. Santra, G. Andria, T.I.M. Ben-Omran, A.B. Chakrapani, E. Crushell, M.J. Henderson, M. Hochuli, M. Huemer, M.C.H. Janssen, F. Maillot, P. D. Mayne, J. McNulty, T.M. Morrison, H. Ogier, S. O'Sullivan, M. Pavlíková, I.T. de Almeida, A. Terry, S. Yap, H.J. Blom, K.A. Chapman, Guidelines for the diagnosis and management of cystathionine beta-synthase deficiency, J. Inherit. Metab. Dis. 40 (2017) 49–74.

[57] D.J. Ham, K.T. Murphy, A. Chee, G.S. Lynch, R. Koopman, Glycine administration attenuates skeletal muscle wasting in a mouse model of cancer cachexia, Clin. Nutr. 33 (2014) 448–458.

[58] E.P.A. Rutten, M.P.K.J. Engelen, A.M.W.J. Schols, N.E.P. Deutz, Skeletal muscle glutamate metabolism in health and disease: state of the art, Curr. Opin. Clin. Nutr. Metab. Care 8 (2005) 41–51.
[59] R.N. Dilger, D.H. Baker, Oral N-acetyl-L-cysteine is a safe and effective precursor of cysteine, J. Anim. Sci. 85 (2007) 1712–1718.
[60] L.F. Ferreira, M.B. Reid, Muscle-derived ROS and thiol regulation in muscle fatigue, J. Appl. Physiol. 104 (2008) 853–860.
[61] I. Medved, M.J. Brown, A.R. Bjorksten, K.T. Murphy, A.C. Petersen, S. Sostaric, X. Gong, M.J. McKenna, N-acetylcysteine enhances muscle cysteine and glutathione availability and attenuates fatigue during prolonged exercise in endurance-trained individuals, J. Appl. Physiol. 97 (2004) 1477–1485.
[62] G. Wu, Y.-Z. Fang, S. Yang, J.R. Lupton, N.D. Turner, Glutathione metabolism and its implications for health, J. Nutr. 134 (2004) 489–492.
[63] I. Ishii, N. Akahoshi, H. Yamada, S. Nakano, T. Izumi, M. Suematsu, Cystathionine gamma-Lyase-deficient mice require dietary cysteine to protect against acute lethal myopathy and oxidative injury, J. Biol. Chem. 285 (2010) 26358–26368.
[64] J.C. Lindon, J.K. Nicholson, E. Holmes, H.C. Keun, A. Craig, J.T.M. Pearce, S. J. Bruce, N. Hardy, S.-A. Sansone, H. Antti, P. Jonsson, C. Daykin, M. Navarange, R. D. Beger, E.R. Verheij, A. Amberg, D. Baunsgaard, G.H. Cantor, L. Lehman-McKeeman, M. Earll, S. Wold, E. Johansson, J.N. Haselden, K. Kramer, C. Thomas, J. Lindberg, I. Schuppe-Koistinen, I.D. Wilson, M.D. Reily, D.G. Robertson, H. Senn, A. Krotzky, S. Kochhar, J. Powell, F. van der Ouderaa, R. Plumb, H. Schaefer, M. Spraul, Standard Metabolic Reporting Structures working group, Summary recommendations for standardization and reporting of metabolic analyses, Nat. Biotechnol. 23 (2005) 833–838.
[65] B.D. Nguyen, X. Meng, K.J. Donovan, A.J. Shaka, SOGGY: solvent-optimized double gradient spectroscopy for water suppression. A comparison with some existing techniques, J. Magn. Reson. 184 (2007) 263–274.
[66] M.H. Stipanuk, P.W. Beck, Characterization of the enzymic capacity for cysteine desulphhydration in liver and kidney of the rat, Biochem. J. 206 (1982) 267–277.
[67] V. Vellecco, A. Mancini, A. Ianaro, V. Calderone, C. Attanasio, A. Cantalupo, B. Andria, G. Savoia, E. Panza, A. Di Martino, G. Cirino, M. Bucci, Cystathionine β-synthase-derived hydrogen sulfide is involved in human malignant hyperthermia, Clin. Sci. (Lond.) 130 (2016) 35–44.
[68] P. De Cicco, E. Panza, C. Armogida, G. Ercolano, O. Taglialatela-Scafati, Y. Shokoohinia, R. Camerlingo, G. Pirozzi, V. Calderone, G. Cirino, A. Ianaro, The hydrogen sulfide releasing molecule acetyl deacylasadisulfide inhibits metastatic melanoma, Front. Pharmacol. 8 (2017) 65.